Colloids and Surfaces A 579 (2019) 123633

Contents lists available at ScienceDirect

Colloids and Surfaces A

journal homepage: www.elsevier.com/locate/colsurfa

Investigation of molecular and mesoscale clusters in undersaturated glycine aqueous solutions

Georgina Zimbitas[a,*], Anna Jawor-Baczynska[a,1], Maria Jazmin Vesga[a], Nadeem Javid[b], Barry D. Moore[c], John Parkinson[c], Jan Sefcik[a,d,*]

[a] Department of Chemical and Process Engineering, University of Strathclyde, 75 Montrose Street, Glasgow, G1 1XJ, UK
[b] School of Chemistry and Biosciences, University of Bradford, Bradford, BD7 1DP, UK
[c] WestCHEM, Department of Pure and Applied Chemistry, University of Strathclyde, 295 Cathedral Street, Glasgow, G1 1XL, UK
[d] EPSRC Future Manufacturing Hub in Continuous Manufacturing and Advanced Crystallisation, University of Strathclyde, 99 George Street, Glasgow, G1 1RD, UK

GRAPHICAL ABSTRACT

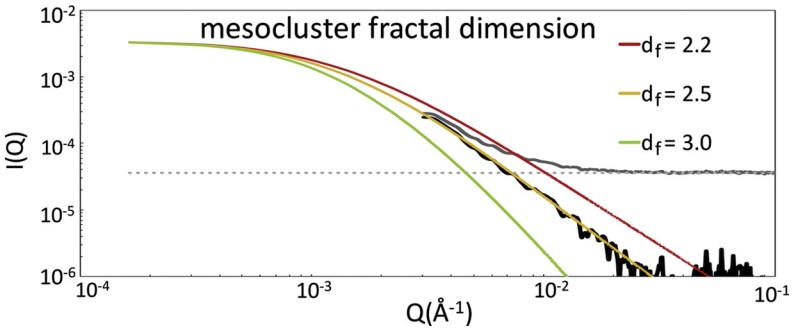

ARTICLE INFO

Keywords:
Clustering
Mesostructured liquid phase
Glycine
Scattering

ABSTRACT

In this work DLS, NTA, SAXS and NMR were used to investigate populations, size distributions and structure of clusters in undersaturated aqueous solutions of glycine. Molecular and colloidal scale (mesoscale) clusters with radii around 0.3-0.5 nm and 100–150 nm, respectively, were observed using complementary experimental techniques. Molecular clusters are consistent with hydrated glycine dimers present in equilibrium with glycine monomers in aqueous solutions. Mesoscale clusters previously observed in supersaturated glycine solutions appear to be indefinitely stable, in mutual equilibrium within mesostructured undersaturated solutions across all glycine concentrations investigated here, down to as low as 1 mg/g of water.

1. Introduction

Aqueous solutions of highly soluble molecules, such as those of small amino acids, are usually assumed to be essentially homogenous systems with some degree of local structuring due to specific interactions on the sub-nanometre scale (e.g. molecular clusters, hydration shells); these molecular structures (molecular clusters) usually do not exceed several solute molecules [1–3]. Such molecular clusters have been reported in both experiments and simulations in aqueous solutions of many organic and inorganic systems [4–10]. In addition to the small molecular clusters, larger colloidal scale (or mesoscale) clusters have also been reported and have been of great interest lately due to

* Corresponding authors.
E-mail addresses: georgina.zimbitas@strath.ac.uk (G. Zimbitas), jan.sefcik@strath.ac.uk (J. Sefcik).
[1] Present address: AstraZeneca, Research and Development, Silk Road Business Park, Charter Way, Macclesfield, SK10 2NA, UK.

https://doi.org/10.1016/j.colsurfa.2019.123633
Received 22 March 2019; Received in revised form 25 June 2019; Accepted 1 July 2019
Available online 02 July 2019

potential roles played by mesoscale structures in crystal nucleation [2,11–15]. Recently published reviews [7,9] emphasize that there are various molecular self-assembly pathways in nucleating solutions and highlight the role of pre-nucleation structures in nucleation of a wide range of organic and inorganic systems.

The presence of sub-micron size domains with liquid-like properties has been widely reported in concentrated solutions of large organic molecules such as proteins [11–13,16–27] as well as in those of smaller molecules [28–41]. Detailed studies of both super- and undersaturated aqueous solutions of NaCl, $(NH_4)_2SO_4$ and Na-citrate, using dynamic light scattering (DLS), revealed that such systems contain not only solvated ions (with radii below 1 nm) but also larger structures with radii varying from 50 nm to 500nm [5]. Using static and dynamic light scattering (SLS and DLS, respectively) further investigation of undersaturated aqueous solutions of common small organic molecules, such as various amino acids and amines [42], citric acid [5,43,44], glucose [44], and urea [43,44], also revealed the presence of large-scale supermolecular structures with broad size distributions, within ranges of several hundred nanometers.

A detailed light scattering study shows that these structures can be characterized as close-to-spherical, discrete domains, which present higher solute density with respect to the less dense remainder of the solution [44–46], with approximately 10^3 to 10^8 solute molecules found to be present in these structures. A study of under- and supersaturated aqueous solutions of DL-alanine revealed mesoscale domains, with radius sizes ranging from 50 nm to 300 nm, existing well below the solid-liquid equilibrium concentration (saturation limit) [10]. These liquid-like, solute-rich mesoscale domains are dispersed within the bulk solution and are not to be considered a separate phase, but instead the liquid phase containing these clusters can be seen as a single liquid phase in thermodynamic equilibrium with the whole system.

The dissolution of glycine crystals in water leads to the formation of an optically clear solution which contains not only a stable population of small molecular clusters, but also contains glycine-rich, liquid-like mesoscale clusters, also referred to as nanodroplets, as observed using SAXS and DLS [10,15]. It has been suggested that the presence of very large nanodroplets, of over 350 nm radius, is required to facilitate crystal nucleation in order to provide the critical mass of glycine essential for productive crystal nucleation [15].

It has been also observed using NTA that mesoscale species were present in undersaturated glycine solutions [17]. However, structure and composition of mesoscale clusters and phase behaviour of such mesostructured liquid phases is very little understood. There has been recently emerging theoretical understanding of thermodynamics of such phases and potential mechanisms of their formation through competing short-range and long-range interactions [47–50], but there is a lack of experimental data on phase behaviour and properties of mesostructured liquid phases.

In this work a range of complementary experimental techniques was used, including Dynamic Light Scattering (DLS), Nanoparticle Tracking Analysis (NTA), Nuclear Magnetic Resonance (NMR), and Small Angle X-ray Scattering (SAXS), to investigate mesostructured glycine solutions over a wide range of glycine concentrations to determine populations, sizes and structures of mesoscale clusters as a function of glycine concentration in aqueous solutions.

2. Experimental methods

2.1. Materials

All chemicals and solvents were of laboratory reagent grade and used without further purification: Glycine puriss. ≥ 99.0%, NT (Fluka), 3-(trimethylsilyl)-2-propionic acid-d4 sodium salt (TSP_d_4) puriss. ≥ 97.0% (Sigma Aldrich), Deuterium Oxide isotopic purity 99.9% (Alfa Aesar). Deionized water was supplied from an in-house Millipore Water System, 18 MΩ/cm and was further filtered using either 0.1 μm (Whatman Cat No 6784-1301) or 1 μm (Whatman Cat. No. 6784-2510) PTFE syringe filters for the preparation of solutions. Concentrations are shown as mg/g and refer to mg of glycine present in g of water.

2.2. Solutions preparation

Aqueous solutions of glycine were prepared by introducing a weighed amount of solid glycine into a known volume of filtered (via PTFE syringe filter) deionized water present in a glass vial with a screw-on cap. Sample solutions were prepared by magnetic stirring for 16 to 24 h within an incubator (constant temperature of 55 °C), with concentrations ranging from 1 to 230 mg/g. Prior to analysis samples were filtered using either 0.1 μm or 1 μm PTFE syringe filters, unless stated otherwise. All syringes, filters, cuvettes and tubes were preheated in the incubator at 55 °C, to avoid premature cooling of the solution during filtering and transfer. NTA and DLS sample cells were preheated to 50–55 °C before the solution was introduced into them and then left to cool to room temperature (18–25 °C), after which they were allowed to equilibrate at room temperature for at least 5 min prior to data collection. Analysis of results required viscosity values of the solvent, and the values used were that of water at the specific analysis temperature, unless stated otherwise. The concentrations used were below the solubility limit of glycine in water, 249.9 mg/g at 25 °C [51], in order to avoid glycine crystallisation.

2.3. Dynamic light scattering (DLS)

DLS measurements were carried out using an ALV/LSE- 5004 instrument, equipped with temperature control at a scattering angle of $\theta = 90^\circ$ and a laser light wavelength of $\lambda = 632.8$ nm. DLS is a well-established experimental technique for studying nanoscale particles in dispersions. By measuring the time-dependent fluctuations of scattered light intensity, arising from Brownian motion, average diffusion coefficients and corresponding hydrodynamic radii can be inferred. Specifically, from the analysis of a measured autocorrelation function the diffusion coefficient of the clusters present was estimated using cumulant analysis [52], and from there the Stokes-Einstein equation was used to derive the hydrodynamic radii, R_h. For DLS measurements, original concentrated solutions were prepared as described above and solutions at lower concentrations were obtained via dilutions of the original solution using filtered Millipore water. Both diluted and original solutions were kept in the incubator at 55 °C, and all DLS measurements were performed between 24 h and 48 h hours after solution preparation. The scattered intensity measured by DLS is shown here in the form of the normalised count rate, NCR, (a.u.), calculated via multiplying the average count rate (kcps) by 10^6 and dividing by the recorded monitor diode value, corresponding to the incident beam intensity.

2.4. Nanoparticle tracking analysis (NTA)

Size distribution and number concentrations of mesoscale clusters were determined using a Nanosight LM10 instrument with a temperature control unit. Nanosight NTA 3 software was used to analyse videos and calculate the size and concentration of clusters. The camera settings of the instrument were set to the 'Autosettings' option, to allow the software to optimize the shutter and gain settings. The sample was introduced into the viewing unit and images of patterns of the laser light scattered by diffusing objects was captured by a CCD camera attached to a microscope. A video was recorded and processed, with each observed individual object 'tracked' by the nanoparticle tracking analysis (NTA) software. Each video was recorded for 60 s and the processing parameters of brightness and gain were optimized by the software. Particle size was calculated from the Brownian motion analysis, whereas the diffusion coefficient was calculated from the mean squared

displacement of the particle tracked. The calculated diffusion coefficient was subsequently substituted into the Stokes-Einstein equation in order to obtain hydrodynamic radii of individual objects tracked. Estimation of the particle concentration was based on the particle count in the illuminated volume ($5.125 \times 10^4\ \mu m^3$) calculated from the dimensions of the field of view (at a magnification of 20x). The total particle count refers to the summation of the particle count up to and including a radius of 250 nm. It has been reported that particle concentration measurements are subject to a variation of up to 25% between identical samples [53].

2.5. Nuclear magnetic resonance (NMR)

Measurements of glycine aqueous solutions were carried out within a Bruker 400 MHz, AV400 Instrument using 16 scans and a relaxation delay of 10 s. The aqueous medium used consisted of a 7:3 H_2O:D_2O w/w ratio. All NMR experiments were conducted using a double coaxial tube system to allow absolute measurement of the glycine concentration: the main sample tube was a Norell 400 MHz, 5 mm diameter, 7″ length NMR tube, whereas the internal reference tube was a Wilmad coaxial insert, stem L32 mm. This setup provided for a sample capacity of 530 µl, and reference capacity of 60 µl. 1 mM of 3-(trimethylsilyl)-2-propionic acid-d4 sodium salt (TSP_d_4) in deuterium oxide was used to provide the internal reference concentration. ^{1}H NMR Diffusion Ordered Spectroscopy (DOSY) measurements were performed at 27 °C (300 K) and results obtained were used for determination of diffusion coefficients of species within the glycine solutions.

2.6. Small angle X-ray scattering (SAXS)

Small angle X-ray scattering measurements were carried out at the SWING beamline at the SOLEIL synchrotron source in Gif-sur-Yvette, France. Aqueous solutions of glycine (ranging from 10 mg/g to 230 mg/g) were prepared at 55 °C and filtered using PTFE 0.1 µm syringe filters. The solutions were injected into a thermostated automatic sample changer and cooled and equilibrated for 5 min at 25 °C. A selected sample would then be automatically passed through a thermostated capillary for exposure to X-ray radiation and detection of scattered intensity patterns. The beam energy was 8 keV and the sample-detector distance was 2.227 m, accessing a Q value range between 0.001 $Å^{-1}$ and 0.17 $Å^{-1}$. Five measurements of a single sample were recorded with an exposure time of 1 s each and 2 s delay time, checked for repeatability and then averaged. The PCCD 170,170 (AVIEX) 2D-detector was present in a vacuum chamber equipped with a pumping system to obtain a primary vacuum of 10^{-6} bar. The vacuum achieved allowed for lower angles to be reached and also reduced the probability of interference from scattering from air molecules. The same measurement procedure was used for pure water samples. The integration and processing of the scattering data was carried out by using the software provided at the beamline.

3. Results and discussion

Following is a report and discussion on the results obtained from Dynamic Light Scattering (DLS), Nanoparticle Tracking Analysis (NTA), Small Angle X-ray Scattering (SAXS), and Nuclear Magnetic Resonance with Diffusion Ordered Spectroscopy (NMR-DOSY) of glycine aqueous solutions within a wide range of glycine concentrations (1–230 mg/g). These solutions were undersaturated with respect to the solubility limit of solid glycine and showed the presence of molecular scale as well as mesoscale clusters across all concentrations investigated. What is reported here is an investigation into the population, size, and structure of the clusters.

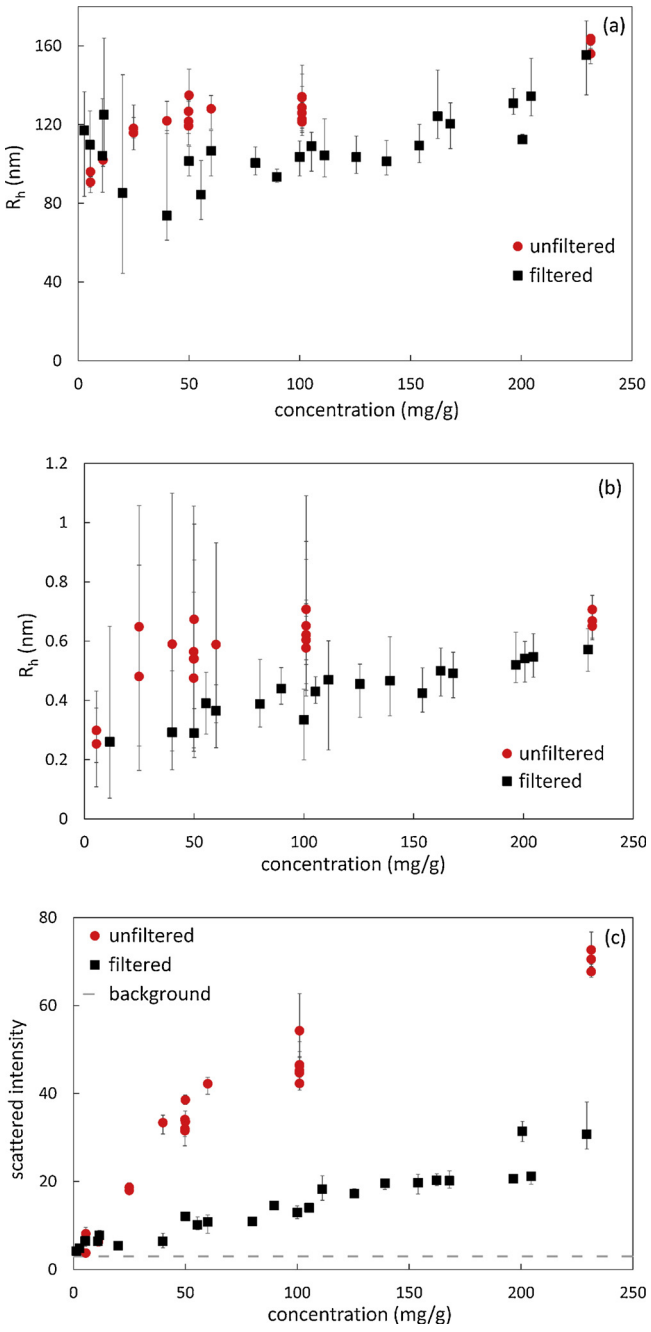

Fig. 1. Hydrodynamic radius R_h (nm) of mesoclusters (a) and molecular clusters (b), and the mean scattered intensity (c) versus the concentration of aqueous glycine solutions. Solutions were either filtered with 1 µm PTFE filters prior to DLS mesurements (black squares), or not filtered at all (red circles).

3.1. DLS measurements

DLS measurement provide us with time averaged scattered intensities and intensity averaged autocorrelation functions, from which mean hydrodynamic radii (R_h) can be estimated using cumulant analysis [52]. The autocorrelation functions measured clearly showed two characteristic decay times (supplementary info, figures S1 & S2), corresponding to a bimodal distribution of species present in glycine aqueous solutions. For filtered solutions, characteristic times of the first decay appeared at times below 0.005 ms, corresponding to molecular clusters, while the second decay appeared at characteristic times over 1 ms, corresponding to mesoscale clusters.

Fig. 1 depicts results from DLS measurements in terms of the mean

hydrodynamic radius of mesoscale clusters (Fig. 1a) and molecular clusters (Fig. 1b), as well as the normalised scattered intensity (Fig. 1c). Two sets of solutions were investigated, with one set using the original concentrated solution unfiltered, and the other set filtering the solution.

The mean mesocluster radius is between 100 and 150 nm, with a slight upward trend at larger glycine concentrations above 150 mg/g (Fig. 1a). At lower glycine concentrations below 50 mg/g there is a larger uncertainty in estimated values as the signal to noise ratio decreases with decreasing concentrations. It can be also seen that unfiltered solutions seem to have somewhat larger mean radii, although these differences are marginal given the accuracy of these estimates, as indicated by the error bars in Fig. 1a. It is interesting to note that the mean size of the mesoclusters varies very little over the whole range of concentrations (1–230 mg/g), which is similar to what was previously observed in DL-alanine aqueous solutions [17].

The mean molecular cluster radius (Fig.1b) for unfiltered solutions varies between 0.3 and 0.5 nm and it increases with increasing glycine concentrations. For unfiltered solutions the mean sizes of molecular clusters seem to be higher but there are large uncertainties in estimated values for lower concentrations up to 100 mg/g but the difference from filtered solutions does not seem to be significant given the errors bars in Fig. 1b. As a radius of the glycine molecule is reported to be 0.28 nm [54], the mean hydrodynamic radius of molecular clusters observed at lower glycine concentrations is in fact consistent with hydrated glycine monomers. As glycine concentration increases, the reversible formation of hydrogen-bonded glycine dimers is increasingly driven by the mass action principle; it was estimated that about 10% of glycine is in the form of a dimer at the highest concentration considered here [55]. The hydrodynamic radius of the glycine dimer is, obviously, larger than that of the glycine monomer. The mean hydrodynamic radius, as measured by DLS, is weighted proportionally to its scattering intensity. This, in turn, is proportional to the cluster mass squared [56,57], which is 4 times that of the monomer. It is therefore expected that the mean hydrodynamic radius of molecular clusters would increase with increasing glycine concentration.

The normalised scattered intensity measured by DLS for filtered and unfiltered solutions is shown in Fig. 1c. A horizontal dashed line shows the background scattered intensity value corresponding to pure water. It can be seen for filtered solutions the scattered intensity increases linearly with glycine concentration between 1 and 230 mg/g. This is different from what was observed in DL-alanine solutions where there appeared to be a critical clustering concentration indicated by a sharp drop off in the scattered intensity at concentrations between 10 and 40 mg/g [17]. However, in glycine solutions the scattered intensity gradually increased across the whole range of concentrations.

The scattered intensity of unfiltered solutions is significantly higher than that of filtered solutions, which means the scattering objects are in greater concentration, and/or they are larger (and thus scattering more strongly) than in filtered solutions. As filter pore sizes (1 μm) are larger than the mean mesoscale cluster diameters, filtration may remove a few very large clusters or break them apart into smaller ones. It may also be that some clusters smaller than the nominal filter pore size become trapped by filters due to their distribution of pore sizes and thus the cluster number concentration is reduced in filtered solutions.

Filtered solutions were also used to create another set of solutions to assess filtration effects: the filtered solutions were either transferred directly into DLS cells without further filtration or filtered into DLS cells using 1 μm PTFE filters (double filtered solutions – supplementary info, Figure S3). Both filtered and double-filtered solutions exhibit similar behaviour, in terms of mean hydrodynamic radii of mesoclusters and molecular clusters, as well as the normalised scattered intensity.

This demonstrated that repeated filtration does not change either size or population of clusters in glycine solutions at a given concentration, although it cannot be ruled out that filtration may disrupt the equilibrium distribution of clusters which then quickly reform under these conditions.

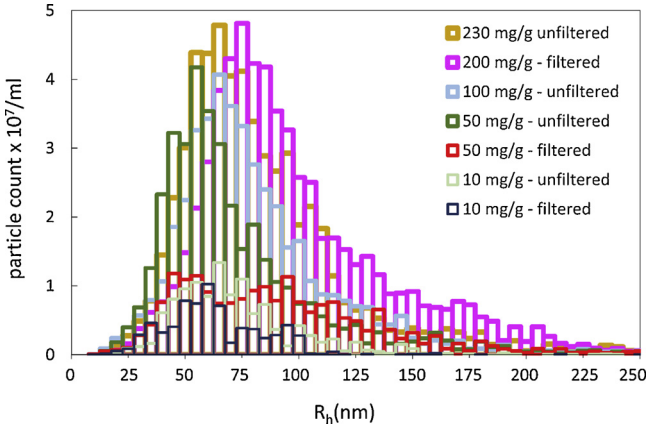

Fig. 2. Number based hydrodynamic radius distributions of mesoscale clusters for selected unfiltered and filtered solutions from NTA measurements.

3.2. NTA measurements

NTA measurements provide us with estimated number concentrations of detected objects and corresponding number-based distribution of hydrodynamic radii of individual objects.

What should be noted here is that the range of the sizes that can be analysed using NTA is reported to be from around 20 nm up to 1 μm (depending on optical contrast material and solvent type), thus precluding the detection of molecular clusters.

Fig. 2 shows the hydrodynamic radius distribution of mesoclusters for unfiltered and filtered glycine solutions of varying concentrations. From these distributions it is evident that while the mode size is similar between 60 and 80 nm for all glycine concentrations, distributions become significantly broader with increasing glycine concentration, with the distribution tail extending towards 250 nm. A comparison of mean hydrodynamic radii of mesoclusters measured by NTA and those measured by DLS is shown in Fig. 3.

While the NTA mean hydrodynamic radius is the number based average, the DLS mean hydrodynamic radius reports the intensity-weighted average [56,57]. The latter is more sensitive towards larger objects, which are weighted proportionally to their mass squared. The intensity weighted average is higher than the number based average unless all objects have the same size, which is not the case here (Fig. 2), and therefore the DLS mean hydrodynamic radius is expected to be higher than the NTA mean hydrodynamic radius as seen in Fig. 3. Furthermore, a small number of large objects would be hardly detected by NTA, which is a technique that provides number-based size

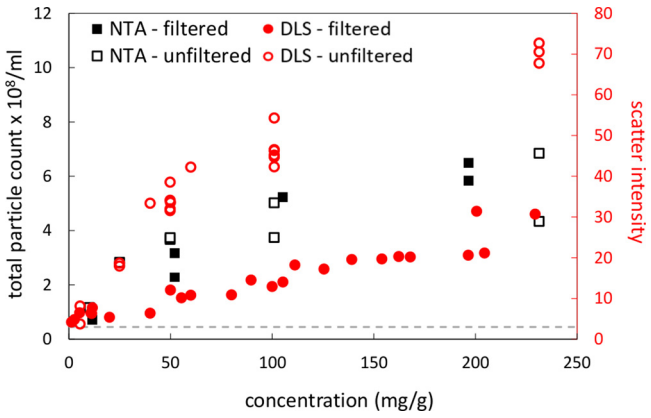

Fig. 3. The total particle count from NTA (black squares) with the overall scattered intensity as obtained using DLS (red circles) for aqueous glycine solutions of different concentrations. DLS results are plotted for filtered (filled symbols) and non-filtered (open symbols) samples.

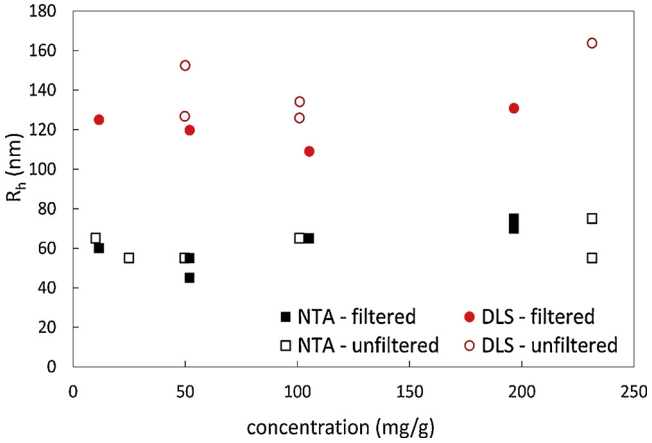

Fig. 4. Mean hydrodynamic radius vs aqueous glycine solution concentration, as measured via NTA (square, black), and DLS (circle, red). Filled symbols represent filtered solutions and open symbols unfiltered solutions. NTA and DLS measurements here were performed on the same day.

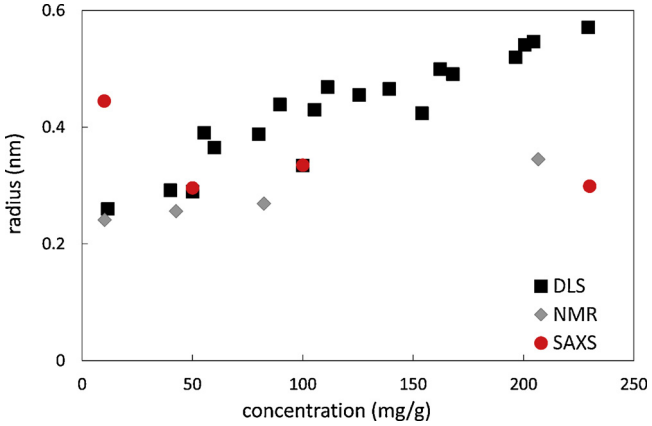

Fig. 5. Radius of gyration R_g from SAXS (red circles) compared to molecular cluster hydrodynamic radius R_h from DLS (black squares) and NMR (grey diamonds) data, for filtered solutions.

distributions via tracking individual objects, while there may, by comparison, be a significant effect on DLS intensity and mean size. This may explain why there is minimal difference between NTA measurements of filtered and unfiltered solutions compared to DLS measurements (Fig. 4 and 5).

In Fig. 3, the scattered intensity measured via DLS is compared to the total number concentration measured via NTA for filtered and unfiltered solutions. The total number concentration increases with glycine concentration, indicating that the scatterer population increases with concentration. The increase in scatterer population is further supported by the fact that for both filtered and unfiltered solutions of the same concentration, the overall particle counts are similar.

3.3. NMR measurements

^{1}H NMR-DOSY measurements provide us with values of diffusion coefficients for species detected by ^{1}H NMR. Measurements were performed with aqueous solutions of glycine at concentrations between 10.2 mg/g and 206 mg/g which correspond to undersaturated conditions in both H_2O and D_2O [58]. The measured diffusion coefficients were similar to those measured in aqueous (H_2O) glycine solutions by Huang et al [55]. The mean hydrodynamic radii of glycine molecular clusters were calculated using the Stokes-Einstein equation and the diffusion coefficient values obtained from DOSY (Table 1), with the viscosity taken as that of a 7:3 H_2O:D_2O w/w mixture at 300 K

Table 1
Diffusion coefficients from DOSY NMR and calculated hydrodynamic diameters for molecular clusters present in aqueous glycine solutions of varying concentrations at 300 K.

concentration (mg/g)	diffusion coefficient x 10^{10} (m^2/s)	Hydrodynamic radius (nm)
206.7	7.0	0.345
82.4	8.96	0.269
42.6	9.42	0.256
10.2	10.0	0.241

(η = 0.91051 cp @ 300 K), with the D_2O viscosity (η = 1.0447 cp at 300 K) determined from values in Millero et al [59] and the H_2O viscosity η = 0, 1.0016 cp at 300 K. From these calculations the hydrodynamic radius was found to vary from 0.241 to 0.345 nm (Table 1 and Fig. 7). Of importance to note is that the mean hydrodynamic radius obtained from NMR-DOSY measurements is a number-based average and when multiple species contribute to the same signal, the NMR signal intensity is proportional to the number of nuclei with the same chemical shift. For example, if a signal comes from both glycine monomer and dimer, it would be proportional to the total number of glycine molecules contained in all monomers and dimers per unit volume.

3.4. SAXS measurements

SAXS measurements provide us with angle dependent scattered intensities I(Q), where the angular dependence is presented in terms of the scattering vector $Q = (4\pi/\lambda)\sin(\theta/2)$, where λ is the beam wavelength and θ is the scattering angle. By recording the elastic scattering of X-rays at low angles, SAXS allows for the acquisition of information about the size and structures of species within a sample that presents inhomogeneities in the nm range. I(Q) data can be analysed to obtain the mean radius of gyration as well as structural information by fitting data with appropriate theoretical form factors.

SAXS measurements were performed with glycine aqueous solutions at concentrations ranging from 10 to 230 mg/g, filtered using 0.1 µm PTFE syringe filters. All SAXS results presented in this work are water background subtracted. SAXS results confirm the presence of small molecular clusters (high Q value) and large mesoscale clusters (low Q value) in undersaturated glycine solutions (Fig. 6), consistent with previous observations from supersaturated glycine solutions [8,12]. This is also in line with results obtained via DLS discussed above.

Guinier analysis was performed in the Q range 0.041-0.29 $Å^{-1}$ (for high Q measurements – see supplementary info). The linear plots are produced by plotting the logarithm of I(Q) against the Q^2, based on the known equation: :

$$\ln[I(Q)] = \ln[Io] - \frac{R_g^2}{3}Q^2 \quad (1)$$

From the linear fit the mean radius of gyration (R_g) for the molecular clusters can be estimated. Fig. 7 shows these radii together with intensities I(Q) for Q = 0.05 (approximating a low Q limit of the scattering intensity for molecular clusters scattering at high Q values) as a function of glycine concentration. The radii are similar to the value from a more concentrated glycine solution (3.6 M) where the mean radius of gyration was reported as 0.34 nm [12]. What must be noted is that for a glycine monomer and dimer, R_g is expected to be around 0.29-0.3 nm and 0.37-0.4 nm, respectively [12].

Fig. 5 shows the mean radii of gyration of molecular clusters obtained from SAXS compared with the respective mean hydrodynamic radii of molecular clusters obtained from DLS and from NMR-DOSY. The radius of gyration is defined as the root mean square of distance from the centre of mass, and is thus expected to be lower than the hydrodynamic radius (for example for a sphere the ratio between the

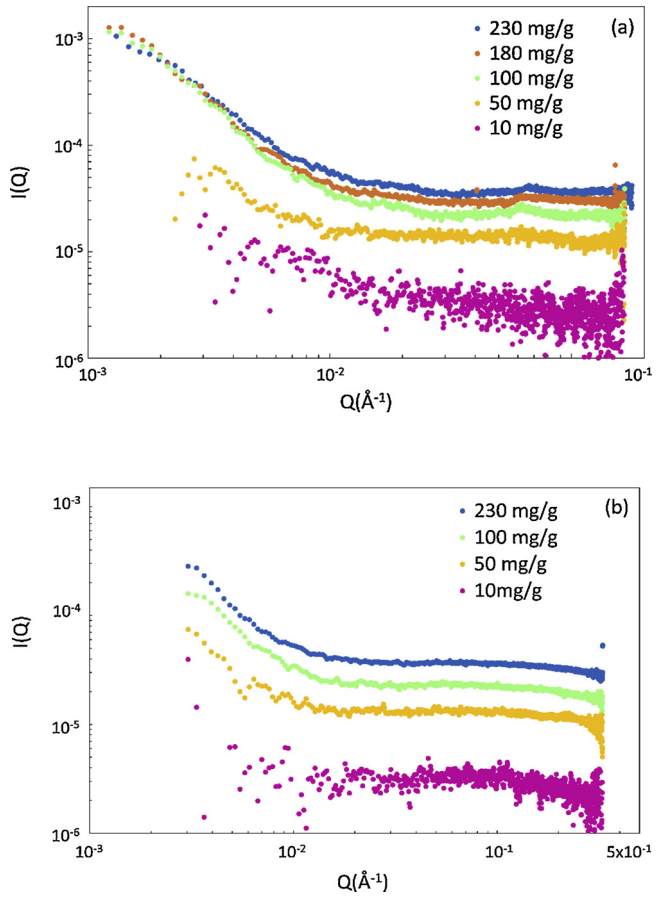

Fig. 6. Variation of scattering intensity I(Q) versus the momentum transfer $Q = 4\pi/\lambda \sin(\theta/2)$ for various concentrations of filtered (0.1 μm PTFE) aqueous glycine solutions. Curves respond from top to bottom to decreasing glycine concentration.
(a) low Q measurement, (b) high Q measurements.

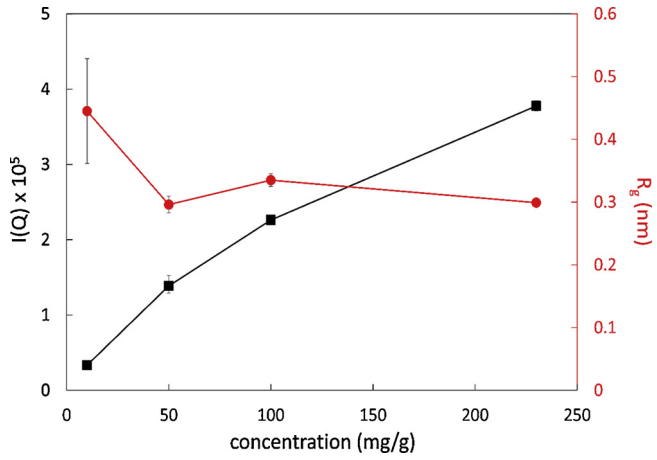

Fig. 7. Variation in SAXS scattering intensity (blacksquares) and radius of gyration R_g (red circles) at $Q = 0.05\,Å^{-1}$ (high Q measurements), over a concentration range of aqueous glycine solutions.

two is $(3/5)^{1/2} = 0.77$). In terms of averaging over multiple species present, the mean radius of gyration is based on species contributions weighted by the species mass squared, similarly to the mean hydrodynamic radius from DLS [56,57]. On the other hand, the mean hydrodynamic radius from NMR-DOSY is based on the species contributions weighted by the number of atoms, i.e., the species mass. Therefore, if only one species is contributing, the mean hydrodynamic radius from DLS and NMR should be close to each other, as is seen at low glycine concentration, where glycine dimers are barely present. As glycine concentration increases and more glycine dimers are formed, the DLS values become higher than the NMR-DOSY values as expected. However, results from SAXS are not consistent with DLS and NMR: while the radius of gyration should be lower than the hydrodynamic radius, it should also increase with increasing glycine concentration due to more dimers forming, however this is not the case. In fact, the radius of gyration from SAXS seems to be close to that expected for the monomer, and at the lowest glycine concentration (10 mg/g) it appears to be too high. This outlier value, however, is subject to significant uncertainty, as can be seen in Fig. 7. In addition, correlations between solute molecule positions can lead to intermolecular interactions which, in turn, induce structure effects, expressed in terms of a structure factor S(Q) [60]. As such there are variations in the observed scattering intensity, $I(Q) = S(Q)P(Q)$, with S(Q) increasingly departing from unity with increasing glycine concentration, thus affecting the apparent radii of gyration estimated from I(Q) data.

SAXS intensity I(Q) corresponding to various structural models was calculated by using experimentally measured size distribution of mesoclusters obtained from NTA, for the entire ensemble of mesoclusters and for the full range of concentrations of analysed glycine solutions. Fig. 8 shows how the mesocluster scattering intensity was obtained from the experimental I(Q) data. The signal relating to mesoclusters (grey solid line) was obtained by subtracting the SAXS intensity at low Q values (signal from both mesoclusters and molecular clusters, experimental data, black solid line) from those at high Q values (signal from molecular clusters, grey dashed line). The specific mesocluster intensity signal is denoted here as $I(Q)_o$ oand defined as the intensity value for the best fit d_f at $Q(Å^{-1}) = 1 \times 10^{-5}$ minus the intensity value of the high Q plateau region value (Table 2 and straight dashed line as seen in Fig. 8). Results for calculated $I(Q)_o$ values for the various concentrations of aqueous glycine solutions measured via SAXS can be found in Table 2. Differences in the $I(Q)_o$ values obtained from high and low Q measurements are mostly due to the fitting of the extrapolation towards $Q(Å^{-1}) = 1 \times 10^{-5}$. The trend, however, is the same in both cases, with the $I(Q)_o$ value decreasing with concentration. The exception here is the value at 230 mg/g, which was calculated using data from unfiltered NTA results, whereas the remaining data were calculated using NTA data from filtered solutions.

Fig. 8 also shows an example of the calculated scattering intensity for both a smooth sphere and a mass fractal model, for a 100 mg/g

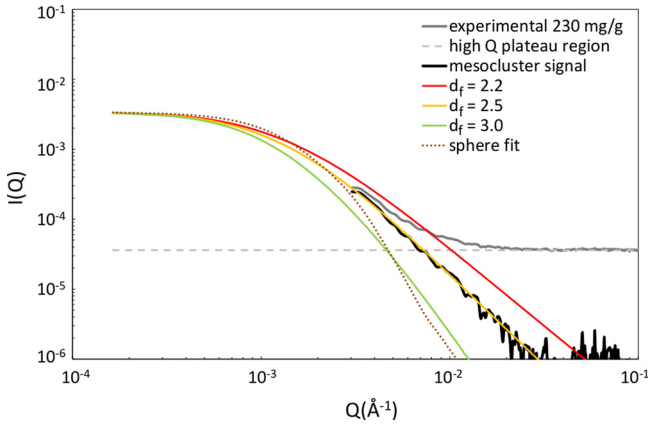

Fig. 8. SAXS experimental data (grey solid line) for a 230 mg/g aqueous glycine solution, plotted with best fits using smooth sphere model (dotted brown line) and the mass fractal model for varying fractal dimension (coloured solid lines), with the best fit being obtained for $d_f = 2.5$. Included in the plot is the scattering from mesoscale clusters (black solid line), as determined after subtraction of the high Q plateau region (dashed grey line) from the low Q region. The slope of the fractal form fit increases with increasing fractal dimension.

Table 2
Fractal dimensions and $I(Q)_o$ for molecular and mesoscale clusters estimated from High and Low Q SAXS data for varying concentrations of aqueous glycine solutions.

concentration (mg/g)	molecular cluster estimated $I(Q)_o$ x 10^5	fractal dimension (d_f)		mesoscale cluster estimated $I(Q)_o$ x 10^3	
		high Q data	low Q data	high Q data	low Q data
230	3.6	2.5	2.2	3.87	2.78
180	2.9	–	2.5	–	4.47
100	2.25	2.5	2.5	4.83	3.38
50	1.35	2.5	2.2	1.09	0.3

glycine aqueous solution. The form factor for a smooth sphere with radius R is given by the following equation:

$$P(Q) = \left[3\frac{(QR) - ((QR)\cos(QR))}{(QR)^3}\right]^2 \quad (2)$$

This model does not have any adjustable parameters and gave a poor fit to the SAXS data, as the slope in the power law region was much less -4, the value expected for smooth spheres. In order to better describe potential cluster structures, an exponential form factor is considered for a mass fractal with radius R and fractal dimension d_f, given by [31]:

$$P(Q) = \frac{sin[(d_f - 1)tan^{-1}(Q\xi)]}{(d_f - 1)Q\xi(1 + Q^2\xi^2)^{\frac{d_f-1}{2}}} \quad (3)$$

where ξ is the cut off, defined as:

$$\xi^2 = \frac{2R^2}{d_f(d_f + 1)} \quad (4)$$

The individual cluster structure factors obtained via intensity-weighted averaging are used in the fractal fit, which was performed using the dimensionless average structure factor [61] employed for experimental data obtained via dynamic and static light scattering:

$$P(Q) = \frac{P(Q)_i N_i m_i^2}{\sum N_i m_i^2} \quad (5)$$

where $m_i = R_i^{d_f}$ is the mass of a cluster with radius R_i, $P(Q)_i$ is the corresponding form factor obtained from Eq. 3 and N_i is the cluster number concentration obtained from NTA. The only adjustable parameter in this model is the cluster mass fractal dimension d_f (cf. Fig. 8).

Overall best fit results for SAXS data obtained for high and low Q data are shown in Table 2, resulting in estimated fractal dimensions between 2.2 and 2.5 for all glycine concentrations where suitable data were available. SAXS data for the lowest glycine concentrations (10 mg/g) were too noisy within the low Q region and as such it was not possible to estimate any properties of mescoscale clusters from SAXS data at these low concentrations.

Fractal clusters have been widely observed in colloidal and biomolecular solutions [62,63]. A fractal dimension of around 2.5 corresponds to fairly compact domains with irregular surfaces and are typical for percolation clusters, while lower fractal dimensions around 2.2 indicate more open structures. This range of fractal dimension indicates that percolation and/or reversible aggregation or restructuring [62] may be responsible for the formation of mesoscale clusters in undersaturated glycine solutions. Higher fractal dimensions of around 2.7, corresponding to more compact, denser structures, were previously estimated for mesoscale clusters in supersaturated glycine solutions [4].

4. Conclusions

Results shown in this work reveal that undersaturated glycine aqueous solutions are mesostructrured liquid phases where hydrated glycine monomer and dimers (molecular clusters) are present alongside mesoscale clusters with radii in the colloidal domain (100–150 nm) across a wide range of glycine concentrations (1–230 mg/g).

Molecular clusters were detected by three complementary experimental methods: DLS, NMR-DOSY and SAXS. Mean hydrodynamic radii of molecular clusters increase with glycine concentration due to an increasing fraction of glycine present in hydrogen-bonded glycine dimers, as shown by both DLS and NMR-DOSY measurements. Surprisingly, the mean radii of gyration from SAXS were found to be independent of glycine concentration, and this discrepancy from the other two methods currently remains unexplained.

Mesoscale clusters were also detected by three separate experimental methods: DLS, NTA and SAXS. Mean hydrodynamic radii of mesoscale clusters were measured by both DLS and NTA, but NTA also provided their cluster size distribution and number concentrations. While mean hydrodynamic radii of mesoscale clusters varied very little with glycine concentrations, their size distributions extended significantly towards larger sizes with increasing glycine concentrations.

Using size distributions and concentrations from NTA measurements, and assuming the mesoscale clusters have mass fractal-like structure, a structural model was developed to fit SAXS data with a single adjustable parameter: the cluster fractal dimension. Using this model fractal dimensions of mesoscale clusters were estimated across a range of glycine concentrations (50–230 mg/g).

Demonstrated in this work is how multiple experimental techniques can be used in conjunction to provide quantitative insights into phase behaviour and properties of mesostructured liquid phases. Self-assembly and nucleation is critically dependent on local compositional and structural heterogeneities within solutions. Developing better experimental and theoretical understanding of complex clustering phenomena in solutions of small molecules is, thus, crucial for further development of rational design and the control of self-assembly and nucleation processes.

Acknowledgments

This project was supported by EPSRC funding via the SynBIM project (Grant Reference EP/P0068X/1) and by the Synchrotron SOLEIL. We would like to thank Dr Javier Perez for his assistance with measurements and raw data analysis at the SWING beamline. The authors would like to declare there are no financial or non-financial competing interests with regards to the work presented in this paper.

Appendix A. Supplementary data

Supplementary material related to this article can be found, in the online version, at doi:https://doi.org/10.1016/j.colsurfa.2019.123633.

References

[1] M.K. Cerreta, K.A. Berglund, The structure of aqueous solutions of some dihydrogen orthophosphates by laser Raman spectroscopy, J. Cryst. Growth 84 (4) (1987) 577–588.
[2] I.T. Rusli, G.L. Schrader, M.A. Larson, Raman spectroscopic study of NaNO3 solution system - solute clustering in supersaturated solutions, J. Cryst. Growth 97 (2) (1989) 345–351.
[3] S.A. Hassan, Morphology of ion clusters in aqueous electrolytes, Phys. Rev. E 77 (3) (2008) 031501.
[4] S. Chattopadhyay, et al., SAXS study of the nucleation of glycine crystals from a supersaturated solution, Cryst. Growth Des. 5 (2) (2005) 523–527.
[5] Y. Georgalis, A.M. Kierzek, W. Saenger, Cluster formation in aqueous electrolyte solutions observed by dynamic light scattering, J. Phys. Chem. B 104 (15) (2000) 3405–3406.
[6] D. Erdemir, et al., Relationship between self-association of glycine molecules in supersaturated solutions and solid state outcome, Phys. Rev. Lett. 99 (11) (2007) 115702.
[7] D. Gebauer, A. Volkel, H. Colfen, Stable prenucleation calcium carbonate clusters, Science 322 (5909) (2008) 1819–1822.
[8] R.J. Davey, S.L. Schroeder, J.H. ter Horst, *Nucleation of organic crystals–a molecular*

perspective, Angew. Chemie Int. Ed. 52 (8) (2013) 2166–2179.
[9] A. Jawor-Baczynska, B.D. Moore, J. Sefcik, Effect of mixing, concentration and temperature on the formation of mesostructured solutions and their role in the nucleation of DL-valine crystals, Faraday Discuss. 179 (2015) 141–154.
[10] A. Jawor-Baczynska, et al., Population and size distribution of solute-rich mesospecies within mesostructured aqueous amino acid solutions, Faraday Discuss. (167) (2013) 425–440.
[11] N. Niimura, et al., Aggregation in supersaturated lysozyme solution studied by time-resolved small angle neutron scattering, J. Cryst. Growth 154 (1) (1995) 136–144.
[12] M. Muschol, F. Rosenberger, Liquid–liquid phase separation in supersaturated lysozyme solutions and associated precipitate formation/crystallization, J. Chem. Phys. 107 (6) (1997) 1953–1962.
[13] C. Haas, J. Drenth, Understanding protein crystallization on the basis of the phase diagram, J. Cryst. Growth 196 (2) (1999) 388–394.
[14] D. Gebauer, et al., Pre-nucleation clusters as solute precursors in crystallisation, Chem. Soc. Rev. 43 (7) (2014) 2348–2371.
[15] A. Jawor-Baczynska, J. Sefcik, B.D. Moore, 250 nm glycine-rich nanodroplets are formed on dissolution of glycine crystals but are too small to provide productive nucleation sites, Cryst. Growth Des. 13 (2) (2013) 470–478.
[16] S. Grouazel, et al., BPTI liquid-liquid phase separation monitored by light and small angle X-ray scattering, Acta Crystallographica Section D 58 (10 Part 1) (2002) 1560–1563.
[17] K. Onuma, N. Kanzaki, Multi-angle static and dynamic light scattering investigation of lysozyme association: from crystallization to liquid–liquid phase separation, J. Cryst. Growth 304 (2) (2007) 452–459.
[18] O. Gliko, et al., A metastable prerequisite for the growth of lumazine synthase crystals, J. Am. Chem. Soc. 127 (10) (2005) 3433–3438.
[19] O. Gliko, et al., Metastable liquid clusters in super- and undersaturated protein solutions, J. Phys. Chem. B 111 (12) (2007) 3106–3114.
[20] V.G. Taratuta, et al., Liquid-liquid phase separation of aqueous lysozyme solutions: effects of pH and salt identity, J. Phys. Chem. 94 (5) (1990) 2140–2144.
[21] C. Ishimoto, T. Tanaka, Critical Behavior of a Binary Mixture of Protein and Salt Water, Phys. Rev. Lett. 39 (8) (1977) 474–477.
[22] O. Galkin, P.G. Vekilov, *Are nucleation kinetics of protein crystals similar to those of liquid droplets?* J. Am. Chem. Soc. 122 (1) (2000) 156–163.
[23] O. Galkin, P.G. Vekilov, *Control of protein crystal nucleation around the metastable liquid–liquid phase boundary*, Proceedings of the National Academy of Sciences of the USA 97 (12) (2000) 6277–6281.
[24] O. Galkin, et al., *Liquid-liquid separation in solutions of normal and sickle cell hemoglobin.* Proceedings of the National Academy of Sciences of the USA 99 (13) (2002) 8479–8483.
[25] O. Galkin, et al., Two-step mechanism of homogeneous nucleation of sickle cell hemoglobin polymers, Biophys. J. 93 (3) (2007) 902–913.
[26] S.T. Yau, B.R. Thomas, P.G. Vekilov, Real time, in-situ, monitoring of apoferritin crystallization and defect formation with molecular resolution, J. Cryst. Growth 232 (1) (2001) 188–194.
[27] L.F. Filobelo, O. Galkin, P.G. Vekilov, Spinodal for the solution-to-crystal phase transformation, J. Chem. Phys. 123 (1) (2005) 014904.
[28] H. Groen, K.J. Roberts, Nucleation, Growth, and Pseudo-Polymorphic Behavior of Citric Acid As Monitored in Situ by Attenuated Total Reflection Fourier Transform Infrared Spectroscopy, J. Phys. Chem. B 105 (43) (2001) 10723–10730.
[29] P.E. Bonnett, et al., Solution crystallisation via a submerged liquid-liquid phase boundary: oiling out, Chem. Commun. (6) (2003) 698–699.
[30] E.L. Heeley, et al., Are metastable, precrystallisation, density-fluctuations a universal phenomena? Faraday Discuss. 122 (2003) 343–361.
[31] T.J. Sorensen, et al., Cluster formation in precrystalline solutions, Chem. Eng. Technol. 26 (3) (2003) 307–312.
[32] S. Veesler, et al., Phase transitions in supersaturated drug solution, Org. Process Res. Dev. 7 (6) (2003) 983–989.
[33] S. Veesler, et al., Crystallization in thepresence of a liquid – liquid phase separation, Org. Process Res. Dev. 10 (4) (2006) 841–845.
[34] L. Lafferrère, C. Hoff, S. Veesler, In situ monitoring of the impact of liquid – liquid phase separation on drug crystallization by seeding, Cryst. Growth Des. 4 (6) (2004) 1175–1180.
[35] L. Lafferrère, C. Hoff, S. Veesler, Study of liquid–liquid demixing from drug solution, J. Cryst. Growth 269 (2) (2004) 550–557.
[36] E. Deneau, G. Steele, An in-line study of oiling out and crystallization, Org. Process Res. Dev. 9 (6) (2005) 943–950.
[37] K. Waizumi, T. Eguchi, Novel observation of nucleation and growth of insulin crystals via liquid droplets generated by liquid–Liquid phase separation, Chem. Lett. 34 (12) (2005) 1654–1655.
[38] M. Kimura, Characterization of the dense liquid precursor in homogeneous crystal nucleation using solution state nuclear magnetic resonance spectroscopy, Cryst. Growth Des. 6 (4) (2006) 854–860.
[39] X. Wang, J.M. Gillian, D.J. Kirwan, Quasi-Emulsion Precipitation of Pharmaceuticals. 1, Conditions for Formation and Crystal Nucleation and Growth Behavior. Crystal Growth & Design 6 (10) (2006) 2214–2227.
[40] K. Kiesow, F. Ruether, G. Sadowski, *Solubility, crystallization and oiling-out behavior of PEGDME: 1. Pure-solvent systems*, Fluid Phase Equilib. 298 (2) (2010) 253–261.
[41] K. Kiesow, F. Tumakaka, G. Sadowski, Experimental investigation and prediction of oiling out during crystallization process, J. Cryst. Growth 310 (18) (2008) 4163–4168.
[42] D. Hagmeyer, et al., Direct experimental observation of the aggregation of α-amino acids into 100-200 nm clusters in aqueous solution, RSC Adv. 2 (11) (2012) 4690–4696.
[43] M. Sedlák, D. Rak, Large-scale inhomogeneities in solutions of low molar mass compounds and mixtures of liquids: supramolecular structures or nanobubbles? J. Phys. Chem. B 117 (8) (2013) 2495–2504.
[44] M. Sedlák, Large-scale supramolecular structure in solutions of low molar mass compounds and mixtures of liquids: I. Light scattering characterization, J. Phys. Chem. B 110 (9) (2006) 4329–4338.
[45] M. Sedlák, Large-scale supramolecular structure in solutions of low molar mass compounds and mixtures of liquids: II. Kinetics of the formation and long-time stability, J. Phys. Chem. B 110 (9) (2006) 4339–4345.
[46] M. Sedlák, Large-scale supramolecular structure in solutions of low molar mass compounds and mixtures of liquids. III. Correlation with molecular properties and interactions, J. Phys. Chem. B 110 (28) (2006) 13976–13984.
[47] M.B. Sweatman, L. Lue, The giant SALR cluster fluid: a review, Adv. Theory Simul. 2 (7) (2019) 1900025.
[48] C.A. Ferreiro-Rangel, M. Sweatman, Cluster formation in binary fluids with competing short-range and long-range interactions, Mol. Phys. 116 (21-22) (2018) 3231–3244.
[49] M.B. Sweatman, L. Lue, The cluster vapor to cluster solid transition, J. Chem. Phys. 144 (17) (2016) 171102.
[50] M.B. Sweatman, R. Fartaria, L. Lue, Cluster formation in fluids with competing short-range and long-range interactions, J. Chem. Phys. 140 (12) (2014) 124508.
[51] R.C. Weast, C.R.C. Handbook of Chemistry and Physics, CRC Press, Cleveland, 1977.
[52] P.N. Pusey, P. Lindner, T. Zemb, Dynamic Light Scattering, in Neutrons, X-rays & Light: Scattering Methods Applied to Soft Condensed Matter, Elsevier Science B.V., 2002 p. 203.
[53] Analytical Software Operation Manual. 2010, NanoSight LM 10 & NTA 2.1.
[54] W.H. Orttung, Polarizability and apparent radius of glycine from refractive index data, J. Phys. Chem. 67 (5) (1963) 1102–1105.
[55] J. Huang, T.C. Stringfellow, L. Yu, Glycine exists mainly as monomers, not dimers, in supersaturated aqueous solutions: implications for understanding its crystallization and polymorphism, J. Am. Chem. Soc. 130 (42) (2008) 13973–13980.
[56] P. Sandkühler, J. Sefcik, M. Morbidelli, Scaling of the kinetics of slow aggregation and gel formation for a fluorinated polymer colloid, Langmuir 21 (5) (2005) 2062–2077.
[57] M.H. Waldner, et al., Initial growth kinetics and structure of colloidal aggregates in a turbulent coagulator, Powder Technol. 156 (2-3) (2005) 226–234.
[58] M. Jelińska-Kazimierczuk, J. Szydłowski, Isotope effect on the solubility of amino acids in water, J. Solution Chem. 25 (12) (1996) 1175–1184.
[59] F.J. Millero, R. Dexter, E. Hoff, Density and viscosity of deuterium oxide solutions from 5-70 °C, Eg, J. Chem. Eng. Data 16 (1) (1971) 85–87.
[60] N. Javid, et al., Protein–protein interactions in complex cosolvent solutions, ChemPhysChem 8 (5) (2007) 679–689.
[61] M. Lattuada, H. Wu, M. Morbidelli, A simple model for the structure of fractal aggregates, J. Colloid Interface Sci. 268 (1) (2003) 106–120.
[62] S. Lazzari, et al., Fractal-like structures in colloid science, Adv. Colloid Interface Sci. 235 (2016) 1–13.
[63] N. Javid, et al., Supramolecular structures of enzyme clusters, J. Phys. Chem. Lett. 2 (12) (2011) 1395–1399.